Optimization of 3D Printing Parameters to Minimize Residual Stresses in Maraging Steel

Karel Trojan[1,a], Ivana Zetková[2,b], Jiří Čapek[1,c], Petr Thurnvald[2,d], Nikolaj Ganev[1,e] and Miloslav Kepka jr.[2,f]

[1]*Faculty of Nuclear Sciences and Physical Engineering, Czech Technical University in Prague; Trojanova 13, 120 00 Prague, Czech Republic;*
[2]*Regional Technological Institute, Faculty of Mechanical Engineering, University of West Bohemia, Univerzitní 8, 306 14 Pilsen, Czech Republic;*

[a]*karel.trojan@fjfi.cvut.cz*, [b]*zetkova@fst.zcu.cz*, [c]*jiri.capek@fjfi.cvut.cz*, [d]*petrt@fst.zcu.cz*, [e]*nikolaj.ganev@fjfi.cvut.cz*, [f]*kepkami1@fst.zcu.cz*

Abstract: During additive manufacturing using the selective laser melting technology, a complex residual stress distribution is created that can significantly affect the printing itself and also the mechanical properties of the final product. Thus, this research has been carried out to optimize 3D printing parameters to minimize residual in maraging steel. It was found that the preheating temperature of the build platform significantly affects both the residual stresses and microstructure parameters as well as the mechanical properties.

Keywords: Additive Manufacturing; Selective Laser Melting; Maraging steel; Residual stresses; Mechanical properties

1 Introduction

Additive Manufacturing (AM), specifically Selective Laser Melting (SLM) technology, is a promising method of metal powder consolidation and offers tremendous opportunities for parts production. This involves selectively melting parts from a thin flat powder bed in layers using a scanning energy source to produce 3D parts. During the SLM process, the sections are heated according to the scanning strategy, allowing independent heating and cooling of the sections, leading to a more complex residual stress (RS) distribution [1]. The magnitude of these RS may even approach the yield strength of the material. The complexity of the SLM process results in the size and orientation of the RS being highly dependent on laser power, scanning speed, scanning strategy, and other printing parameters.

Fatigue crack initiation and propagation play an important role in fatigue properties, where they are shown to be strongly associated with surface roughness, microstructure parameters (dislocation density, crystallite size, microcracks) and RS [2]. In a study [3], the correlation between the initiation and propagation of surface fatigue cracks with RS was investigated in laser-welded materials using X-ray diffraction, where it was found that not only RS, but also the distribution of microstructure parameters, plays a crucial role in fatigue. In general, the distribution of RS in AM specimens is highly dependent on the printing strategy. The distribution of internal RS is crucial for the deformation of the sample and the formation of fatigue cracks. Therefore, this research was conducted to minimize the RS of 3D printed maraging steel.

2 Experiment

An EOS M290 machine with the printing parameters shown in Table 1 was used to produce 5 mm diameter test specimens of C300 maraging steel (trademark MS1), see Table 2 for chemical composition. Research has been carried out on what changes in the process parameters lead to a reduction in RS after solution annealing heat treatment at 820°C without

following machining. The most significant effect was to change the setting of preheat of the building platform from the default 40°C to 120°C. Therefore, two samples were analysed, where the sample marked SP had a preheating temperature of 40°C and the sample P120 a temperature of 120°C.

Table 1. Infill printing parameters.

Parameter	
Laser power	285 W
Laser speed	960 mm/s
Hatch distance	110 µm
Layer thickness	40 µm
Printing strategy pattern	Stripes

Table 2. Chemical composition of C300 maraging steel (trademark MS1) [4].

Element	Composition [wt.%]
Ni	17–19
Co	8.5–9.5
Mo	4.5–5.2
Ti	0.6–0.8
Al	0.05–0.15
Cr, Cu	each ≤ 0.5
C	≤ 0.03
Si, Mn	each ≤ 0.1
P, S	each ≤ 0.01
Fe	Bal.

Macroscopic RS were determined from the centre of the cylindrical test samples using X-ray diffraction. The RS values were calculated from lattice deformations determined on the basis of experimental dependencies of $2\theta(\sin^2\psi)$ assuming a biaxial state of residual state of stress (θ is the diffraction angle, ψ the angle between the sample surface and the diffracting lattice planes). The diffraction angle was determined as the centre of gravity of the Cr$K\alpha_1\alpha_2$ doublet diffracted by the lattice planes {*211*} of the α-Fe phase. The X-ray elastic constants $\frac{1}{2}s_2$ = 5.76 TPa^{-1}, s_1 = –1.25 TPa^{-1} were used for the stress calculation. The experimental error is the standard deviation according to the "$\sin^2\psi$" residual stress calculation algorithm. The FWHM value (Full Width at Half Maximum) was determined from the analysed diffraction line {*211*} at a tilt of $\psi = 0°$, the error of determination does not exceed 0.05° 2θ. The depth profile of RS, which was determined in the direction of the axis of the cylindrical test specimen, was obtained by gradual electrolytic removal of the surface layers.

Tensile tests were carried out on the FU250_AH250 tensile testing machine, which is equipped with an extensometer. From the data obtained, the ultimate strength, the yield strength corresponding to 0.2% of plastic strain and the elongation at break were evaluated. All results of mechanical properties shown, see Table 3, are the average of at least two values.

3 Results

From the results of macroscopic RS, obtained from the centre of the cylindrical test samples, it is clear that the depth profile varies significantly from sample to sample, see Fig. 1. Tensile RS still dominate in the near vicinity of the surface for both samples, however, for sample P120 (120°C platform preheating) a rapid decrease of RS can be observed with only compressive residual stresses being described with a maximum at a depth of about 120 µm. On the contrary, the RS for sample SP (default platform preheating, i.e. 40 °C) show a tensile character up to a depth of 170 µm with a maximum of more than 300 MPa. This state of RS is unfavourable as high tensile values reduce the yield stress and promote crack initiation and their growth. However, at greater depths for the SP sample, compressive RS have also been

described. The high tensile RS in the surface layers did not affect the strength, as the ultimate tensile strength for the SP specimen is approximately 50 MPa higher than for P120, see Table 3. There could be a greater effect on fatigue life, but the surface tensile RS of specimen P120 probably explains one of the reasons why there was no increase in fatigue life between specimen P120 and SP (results will be the subject of another article). Therefore, further print optimisation will be required to minimize surface RS.

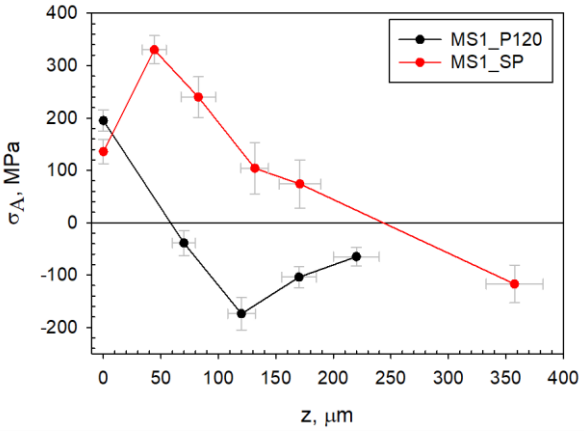

Fig. 1 Depth profile of macroscopic residual stresses.

Fig. 2 shows the depth profile of the FWHM parameter, which is the width at half of the observed diffraction maximum. From the increasing value of FWHM, it could be said that in the analysed volume the crystallites (coherent diffracting domains) are smaller and/or the microstrain (deformation of individual crystallites) is higher. From the comparison, it can be clearly stated that in the surface layers of the P120 sample, the crystallite size is smaller and/or the microstrain value is higher. Thus, if we compare these conclusions with the results of mechanical properties (see Table 3), it is not surprising that the sample P120 shows lower extensibility and higher yield strength, since the value increases with increasing microstrain (which is due to a higher dislocation density) and with decreasing grain size d (according to the Hall-Petch effect following a $d^{-½}$ relationship), since the crystallite size often correlates with the grain size. The values of yield strength and tensile strength are within error identical to those given in the material data sheet of the powder manufacturer (see Table 3), solution heat treatment had no significant effect on the mechanical properties.

Table 3. Comparison of the obtained mechanical properties (solution heat treatment at 820°C) with tabulated values for as-build state [4].

	MS1_SP	**MS1_P120**	**Tabulated values**
Yield strength, MPa	879 ± 14	916 ±7	930 ± 150
Ultimate tensile strength, MPa	1120 ± 1	1069 ± 2	1100 ± 150
Elongation at break, %	15	12	12 ± 4

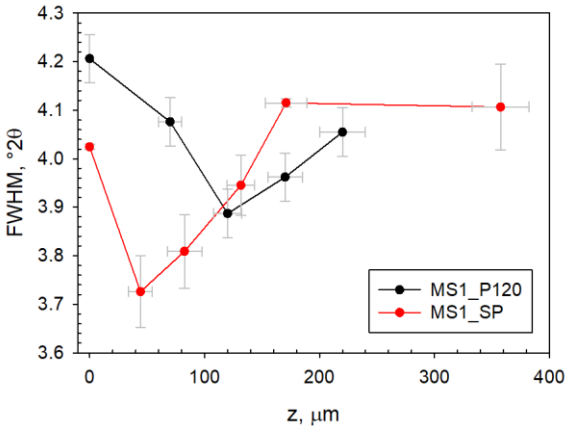

Fig. 2 Depth profile of the FWHM parameter.

Conclusions

It was found that increasing the temperature of the printing platform to 120 °C significantly affected the residual stresses after heat treatment of the printed samples by SLM. The samples with different preheating temperatures also differed in mechanical properties. Further optimization of the printing parameters is needed to minimize the residual stresses also on the surface. This should have a pronounced effect on improving the material properties, especially the fatigue life.

Acknowledgements

The work was supported by Technology Agency of the Czech Republic "Development of "3D print-thermal spray" systems for dynamically and cyclically loaded applications", grant No. TH75020003. The work of CTU staff was supported by the Grant Agency of the Czech Technical University in Prague, grant No. SGS22/183/OHK4/3T/14.

References

[1] Bartlett, J. L. and Li, X. "An overview of residual stresses in metal powder bed fusion," *Additive Manufacturing*, **27**, pp. 131-149 (2019).

[2] Schneller, W., Leitner, M., Pomberger, S., Springer, S., Beter, F. and Grün F. "Effect of post treatment on the microstructure, surface roughness and residual stress regarding the fatigue strength of selectively laser melted AlSi10Mg structures," *Journal of Manufacturing and Materials Processing*, **3**(4), 89 (2019).

[3] Černý, I., Čapek, J., Kec, J., Trojan, K., Ganev, N. and Němeček, S. "Fatigue of Laser-Welded Structures: Role of Residual Stress," in *Comprehensive Structural Integrity*, Aliabadi F. and Soboyejo W., ed. (Elsevier Science, 2023).

[4] EOS GmbH - Electro Optical Systems, "EOS MaragingSteel MS1 – Material data sheet," *Available from* https://www.eos.info/03_system-related-assets/material-related-contents/metal-materials-and-examples/metal-material-datasheet/werkzeugstahl_ms1_cx/ms1/ms-ms1-m280_m290_400w_material_data_sheet_07-22_en.pdf *Accessed:* 2023-05-15.